SCIENCE CHINA
Chemistry

•ARTICLES•

May 2021 Vol.64 No.5: 861–872
https://doi.org/10.1007/s11426-020-9940-6

Remote, selective, and *in situ* manipulation of liquid droplets on a femtosecond laser-structured superhydrophobic shape-memory polymer by near-infrared light

Xue Bai, Jiale Yong, Chao Shan, Yao Fang, Xun Hou & Feng Chen*

State Key Laboratory for Manufacturing System Engineering and Shaanxi Key Laboratory of Photonics Technology for Information, School of Electronic Science and Engineering, Xi'an Jiaotong University, Xi'an 710049, China

Received November 24, 2020; accepted January 13, 2021; published online March 15, 2021

Droplet manipulation plays a significant role in the fields of biomedical detection, microfluidics, and chemical engineering. However, it still remains a great challenge to simultaneously achieve remote, selective, and *in situ* droplet manipulation on the same surface. Here, Fe_3O_4 nanoparticles were doped in a shape-memory polymer (SMP) to prepare a photothermal-responsive Fe_3O_4-SMP composite which showed remarkable near-infrared (NIR) light-triggered shape-memory property. Superhydrophobic micropillar array was constructed on such Fe_3O_4-SMP composite through femtosecond laser microfabrication and fluoroalkylsilane modification. The surface wettability of the as-prepared surface can transform from a low-adhesive sliding state to a high-adhesive pinning state as the micropillars are deformed by pressing. Interestingly, the deformed micropillars can stand up and restore to their original morphology under remote NIR light irradiation, resulting in the reversible and repeatable recovery of the ultralow-adhesive superhydrophobicity. With such light-triggered wettability switching, the droplets pinning on the sample surface can be remotely, selectively, and *in situ* released. Furthermore, the superhydrophobic Fe_3O_4-SMP surface is successfully applied in lossless liquid transfer, selective droplet release, and droplet-based microreactor. The as-fabricated superhydrophobic surfaces with NIR light-controlled reversible wettability will hold great promise in the fields of liquid manipulation, lab-on-a-chip, and microfluidics.

droplet manipulation, superhydrophobicity, shape-memory polymer, femtosecond laser, light responsive

Citation: Bai X, Yong J, Shan C, Fang Y, Hou X, Chen F. Remote, selective, and *in situ* manipulation of liquid droplets on a femtosecond laser-structured superhydrophobic shape-memory polymer by near-infrared light. *Sci China Chem*, 2021, 64: 861–872, https://doi.org/10.1007/s11426-020-9940-6

1 Introduction

Droplet manipulation has aroused increasing attention because of its broad applications in droplet transfer [1–3], biological monitoring [4–6], lab-on-a-chip [7,8], and microfluidic devices [9–11]. Superwetting surfaces have been widely used in droplet manipulation [12–16]. Like the lotus leaf and rose petal in nature, superhydrophobic surfaces can exhibit different dynamic wettabilities, such as ultralow water adhesion and ultrahigh water adhesion [2,17]. Water droplets roll off easily on the lotus leaf. Such low-adhesive superhydrophobic surfaces usually have excellent self-cleaning ability. By contrast, rose-petal-like superhydrophobic surfaces show high water adhesion, which can be functionalized as a "mechanical hand" to grasp and transport small water droplets. For example, Cheng *et al.* [18] fabricated a sticky superhydrophobic polydimethylsiloxane (PDMS) film by the combination of electrodeposition and casting replication technique. The water droplet could strongly attach to the sample surface; thereby the droplet was transported from a low-adhesive superhydrophobic surface to a higher-adhesive superhydrophobic

*Corresponding author (email: chenfeng@mail.xjtu.edu.cn)

© Science China Press and Springer-Verlag GmbH Germany, part of Springer Nature 2021

surface by using this sticky superhydrophobic surface, without any mass loss. Liu *et al.* [19] also achieved the non-loss transfer of water droplet by the superhydrophobic copper surface with high water adhesion. Lee *et al.* [20] fabricated a high-adhesive superhydrophobic nanowire array to achieve droplet transfer and mixture. By using the high-adhesive superhydrophobic surfaces, water droplets can be transported from a lower-adhesive surface to a higher-adhesive surface, but such transfer process is irreversible. The reported sticky superhydrophobic surfaces can only release a droplet to a substrate with a higher adhesion and cannot achieve *in situ* droplet release. For practical applications, it is greatly desirable to realize *in situ* reversible droplet manipulation on a single sample surface. Sun *et al.* [21] developed a novel superhydrophobic PDMS micropillar array whose wettability could be reversibly switched between sliding state and pinning state by tuning the surface curvature. The water adhesion of the surface gradually decreased with increasing the surface curvature, and thereby the water droplets could be *in situ* released as the curvature exceeded a critical value. Shape-memory polymer (SMP) is an important class of smart materials that can reversibly change its shape between permanent state and temporary state upon external environment [22,23]. Such shape-recoverable substrate provides a potential candidate to reversibly tune the surface wettability (*e.g.*, switchable water adhesion) by regulating the morphology of SMP microstructures [24–27]. For example, Liu *et al.* [24] prepared a superhydrophobic surface by constructing micropillar structures on the SMP substrate. The wettability of the surface can be reversibly switched between the sliding state and the pinning state through alternate pressing and heating the micropillars. Recently, Wu *et al.* [28] integrated a superhydrophobic SMP microcone array with a silver nanowire heater circuit. The wettability of the surface could be *in situ* transformed between sliding state and pinning state under circuit heating, thus realizing the *in situ* release of water droplets. Although the abovementioned smart surfaces can achieve droplet release *in situ*, the triggering process must be operated at a very near distance and it is difficult to selectively manipulate specific droplets on a sample surface. As a typical noncontact manner, remote manipulation enables high spatial and temporal controllability [23,29–31]. Simultaneously achieving remote, selective, and *in situ* manipulation of liquid droplets on a superhydrophobic surface is of great significance to broaden the application fields of droplet manipulation technology in practice, and to date, such methods and surfaces have been rarely reported.

In this study, Fe_3O_4 nanoparticles were doped into a thermal-responsive SMP matrix to endow the SMP composite with photothermal responsive property. Micropillar array was prepared on the surface of the Fe_3O_4-SMP composite by femtosecond laser processing, which showed low-adhesive superhydrophobicity after fluoroalkylsilane modification. The micropillars could be inclined upon pressing treatment and recover to original state just by near-infrared (NIR) light irradiation. As a result, the surface wettability was reversibly transformed between low-adhesive superhydrophobic state and high-adhesive pinning state. Water droplets pinning on the sample surface could be remotely, selectively, and *in situ* released by NIR light irradiation. Based on the unique light-triggered wettability transformation, lossless liquid transfer, selective liquid release, and droplet-based microreactor were achieved by using the superhydrophobic Fe_3O_4-SMP surface.

2 Experimental

2.1 Preparation of the Fe_3O_4-SMP composite

The blank SMP resin matrix was prepared by thoroughly mixing the diglycidyl ether of bisphenol A (Nantong Xingchen Synthetic Material Co., Ltd., China), *n*-octylamine (J&K Scientific Ltd), and *m*-xylylenediamine (J&K Scientific Ltd., China) at a molar ratio of 5:1:2. Then, the Fe_3O_4 nanoparticles (with a diameter of 200–300 nm, Aladdin Industrial Corporation, USA) were dispersed into the SMP resin matrix with mechanically stirring for about 10 min, as shown in Figure 1(a). After degassing treatment, the dispersion was poured into a Teflon mold and successively cured at 60 °C for 2 h and then at 100 °C for 1 h to obtain the Fe_3O_4-SMP composite, as shown in Figure 1(b, c).

2.2 Formation of micropillar array

Femtosecond laser processing was utilized to generate micropillars on the Fe_3O_4-SMP surface. The laser pluses (a pulse width of 50 fs, a central wavelength of 800 nm, and a repetition rate of 1 kHz) were produced from a Ti:sapphire laser system (Libra-USP-HE, Coherent, USA) and were focused onto sample surface *via* an objective lens (×5, NA=0.15, Nikon, Japan). The whole surface of the Fe_3O_4-SMP substrate was firstly processed by a femtosecond laser at the laser power of 10 mW, the scanning speed of 6,000 μm/s, and the interval of scanning lines of 6 μm. Then, the Fe_3O_4-SMP surface was selectively ablated by femtosecond laser to create micropillar array. As shown in Figure 1 (d), the orthogonally-crossed femtosecond laser line-by-line ablation manner was exploited. The interval of scanning lines was adjusted from 2 to 10 μm, the laser power was adjusted from 30 to 70 mW, and the scanning speed was constant at 4,000 μm/s. During the femtosecond laser processing, the laser selectively ablated the sample surface. The ablated region was lower than the untreated region because of the laser-induced material removal, so the rest untreated region finally developed to a micropillar array on the Fe_3O_4-SMP composite. After ultrasonically cleaning, the laser-

structured samples were fluorinated by placing in a closed container together with several drops of 1*H*,1*H*,2*H*,2*H*-perfluorodecyltrichlorosilane (Aladdin Industrial Corporation) for 4 h at room temperature.

2.3 Manipulation of the micropillar array

The NIR light (wavelength=808 nm, FU808AD2000-F34, Shenzhen Fuzhe Technology Co., Ltd., China) was used to irradiate the sample, which makes the micropillar-structured Fe_3O_4-SMP composite become soft. Then, the soft sample was pressed by a flat surface to cause the micropillars lean to one side. Under the pressure, the composite was cooled down to fix the deformed shape of the micropillars. The recovery of the micropillar morphology was simply realized by a NIR light re-irradiation process.

2.4 Characterization

A thermal infrared camera (VarioCAM®) was used to measure the surface temperature of the Fe_3O_4-SMP composite under NIR light irradiation. Dynamic mechanical analysis (DMA) (DMA242E, Netzsch) was exploited to characterize the storage modulus and tanδ of the sample. The surface morphology was observed by a scanning electron microscope (SEM) (FlexSEM-1000, Hitachi, Japan). The values of contact angle (CA) and sliding angle (SA) were obtained by a contact angle measurement (JC2000D, PoweReach) with the water volume of 6 μL.

3 Results and discussion

3.1 Preparation and property of the Fe_3O_4-SMP composite

Introducing light-absorbing additives into the thermal-responsive SMP is a common method of preparing photo-responsive SMP [32–34]. The epoxy-based SMP used here is a typical thermal-responsive polymer, whose shape can recover from deformed state to original state above its glass transition temperature (T_g). Light can travel a very long distance and can be easily converted into heat energy. Fe_3O_4 nanoparticles can absorb photon energy and convert it into thermal energy, thereby increasing the sample temperature [35]. To endow the thermal-responsive SMP matrix with photothermal responsive property, Fe_3O_4 nanoparticles were introduced into such SMP substrate, as shown in Figure 1(a–c). A certain amount of Fe_3O_4 nanoparticles were added into the mixture of the SMP prepolymer and curing agent, and thoroughly stirred to form a homogeneous dispersion (Figure 1(a)). Then the dispersion was carefully poured into a shallow groove on a Teflon mold, which was pre-placed in a vacuum oven in order to completely remove air bubbles in the dispersion (Figure 1(b)). The dispersion was cured by heating treatment at 60 °C for 2 h and then at 100 °C for 1 h. Finally, the solid Fe_3O_4-SMP composite was obtained by peeling off from the mold (Figure 1(c)).

As a typical photothermal conversion material, black Fe_3O_4 nanoparticles have strong light-absorption ability in the NIR spectrum [36–39]. Under NIR light irradiation, Fe_3O_4 nanoparticles can absorb light energy and immediately convert into thermal energy, which is well known as the photothermal effect [40–42]. As shown in Figure 2(a), the thermal image indicates that NIR light irradiation can increase the surface temperature of the Fe_3O_4-SMP composite. With extending the irradiation time, the surface temperature of the sample gradually increases. The content of Fe_3O_4 nanoparticles has a great influence on the photothermal behavior of the composite. After NIR light irradiation (light intensity: 1.7 W/cm^2, irradiation distance: 45 cm) for 10 s, the surface temperatures of different samples with 0.2 wt%, 1 wt%, 2 wt%, and 4 wt% Fe_3O_4 nanoparticles reached up to 78, 108, 137, and 140 °C, respectively (Figure 2(b)). The results indicate that a SMP composite with higher Fe_3O_4 nanoparticle content tends to have a higher surface temperature under the same light irradiation time. The photothermal ability of the 2 wt% Fe_3O_4-SMP composite is close to that of the 4 wt% Fe_3O_4-SMP composite, so the Fe_3O_4-SMP composite with 2 wt% Fe_3O_4 nanoparticles was used in subsequent experiment.

DMA is usually utilized to measure the thermal and mechanical properties of a polymer. From the tanδ curve in Figure 2(c), it can be found that the T_g of the blank SMP is about 56 °C. The addition of Fe_3O_4 nanoparticles makes the T_g of the resultant Fe_3O_4-SMP composite decrease to 53 °C. Such slight T_g decline is attributed to the fact that the doped nanoparticles hinder the crosslinking of the SMP molecular chains to some extent during the polymerization process [35]. As the temperature increases from 20 to 80 °C, the phase state of the polymer will dramatically change from glassy state to rubbery state, and thus the storage modulus of the blank SMP declines from 3.3 GPa to 3.1 MPa while that of the Fe_3O_4-SMP composite declines from 3.9 GPa to 1.3 MPa (Figure 2(c)). The blank SMP and the Fe_3O_4-SMP composite have approximate equivalent T_g and storage modulus, so the doping of Fe_3O_4 nanoparticles has little effect on the thermal and mechanical properties of the SMP substrate.

To demonstrate the photo-responsive ability of the Fe_3O_4-SMP composite, a composite with the dimension of 33 mm ×4.3 mm×1.3 mm (length×width×thickness) was heated and stretched up to 27% strain and then immediately cooled down to lock the deformed shape (Figure 2(e, f)). A blank SMP with the same dimension was used as a comparison group. Upon NIR light irradiation (light intensity: 2.6 W/cm^2, irradiation distance: 30 cm), the stretched Fe_3O_4-

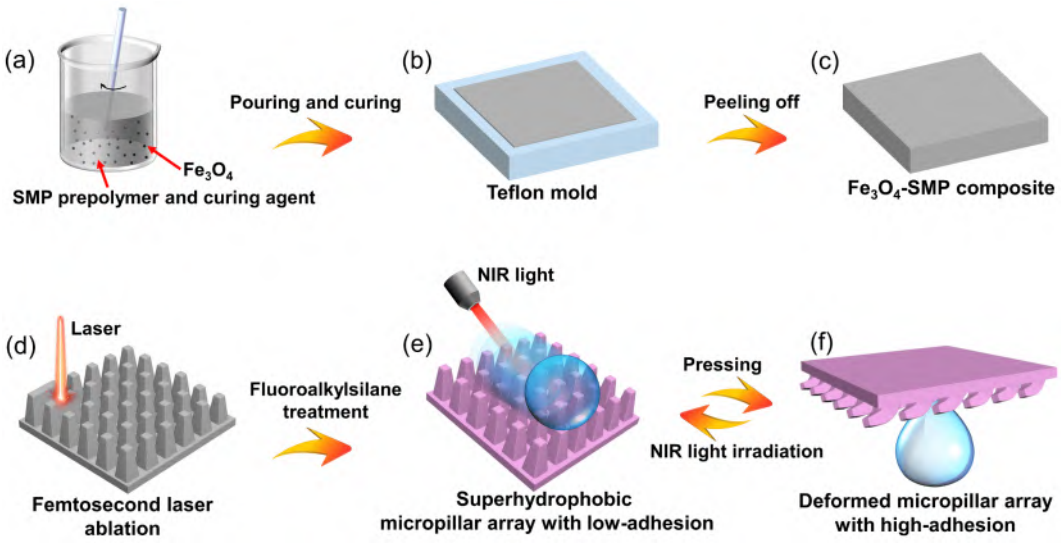

Figure 1 Illustration of the preparation process of the superhydrophobic Fe_3O_4-SMP micropillars with NIR light-triggered reversible wettability. (a–c) Preparation process of the Fe_3O_4-SMP composite. (d) Preparation of micropillars on the Fe_3O_4-SMP composite by femtosecond laser. (e, f) Reversible switching of wettability between sliding state and sticky state through pressing and NIR-light irradiation processes (color online).

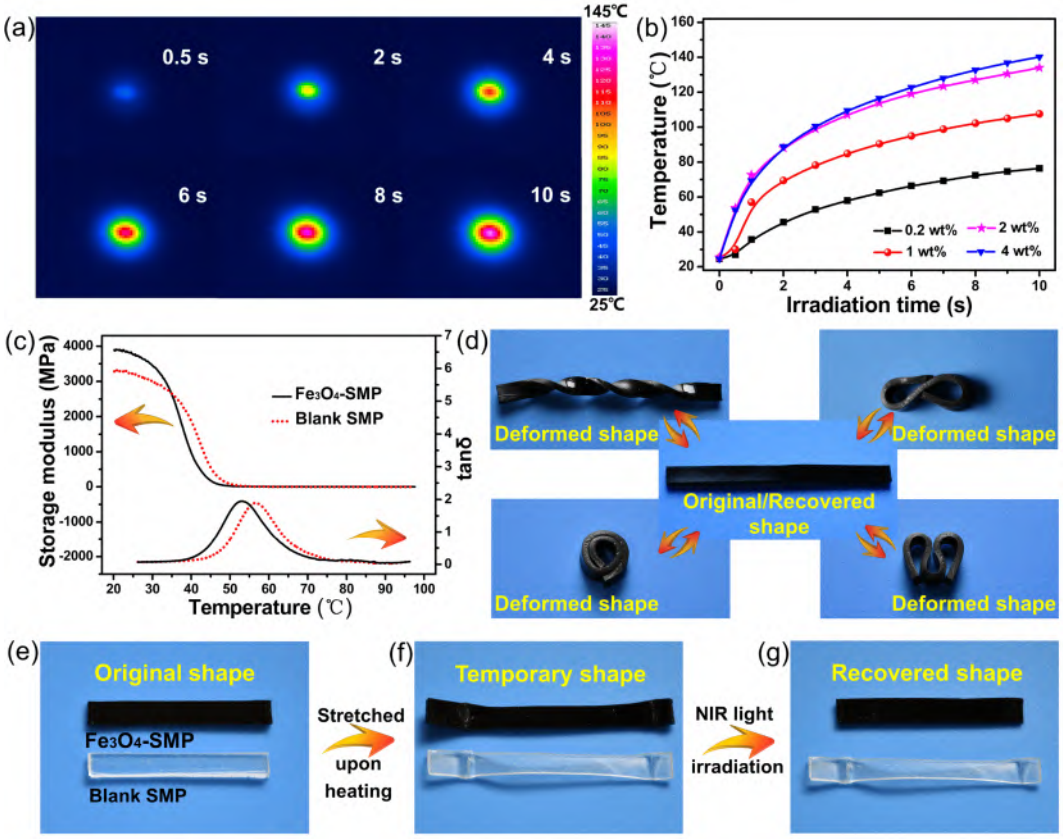

Figure 2 Photothermal effect and shape-memory ability of the Fe_3O_4-SMP composite. (a) Thermal images of irradiating a Fe_3O_4-SMP composite by NIR light for different time. (b) Influence of the content of Fe_3O_4 nanoparticles on the photothermal behavior of the Fe_3O_4-SMP composites. (c) DMA curves for the Fe_3O_4-SMP composite and the blank SMP. (d) Reversible deformation and recovery of the Fe_3O_4-SMP strip between original shape and various deformed shapes. (e–g) Deformation and recovery of the Fe_3O_4-SMP composite under stretching and light irradiation treatments. The blank SMP is used as a control sample (color online).

SMP composite could recover to its original length immediately (Figure 2(g)). In contrast, the blank SMP maintained the stretched state even after continuous NIR light exposure for some minutes (Figure 2(g)). Therefore, the

doping of Fe_3O_4 nanoparticles enables the SMP composite to have excellent photo-responsive ability. In addition to the simple stretching deformation, the Fe_3O_4-SMP composite could also be temporarily programmed into other different complex shapes, such as the twisted shape, "∞" shape, circle shape, and "M" shape (Figure 2(d)). The composite with various temporary shapes could completely restore to its original shape *via* NIR light irradiation because of the excellent photo-responsive shape-memory property of the Fe_3O_4-SMP composite (Figure 2(d)).

3.2 Superhydrophobic microstructure and wettability switching

Femtosecond laser direct writing is utilized to prepare the micropillar structures on the Fe_3O_4-SMP composite *via* an orthogonally-crossed line-by-line ablation method [15,16,31] (Figure 1(d)). During the scanning process, the adjacent laser-pulse-induced craters were strongly overlapped, thus resulting in the dramatic material removal. As a result, the ablated region is lower than the untreated region. The preprogramed rectangular scanning path can be precisely controlled by a computer program. Through selective femtosecond laser scanning, the laser-ablated region develops to the rectangular microgroove-patterned structure on the Fe_3O_4-SMP composite. The rest untreated region naturally becomes the ridge structures between adjacent microgrooves. After that, the sample is rotated by 90° in the *X*-*Y* plane and the abovementioned selective femtosecond laser scanning process is repeatedly executed. The remaining unablated region finally forms the micropillar array structure on the sample surface.

Figure 3(a, b) display the SEM images of the femtosecond laser-structured micropillar array. The micropillar array was prepared at the laser power of 40 mW, the scanning speed of 4 mm/s, and the interval of scanning lines of 2 μm. The as-prepared micropillars have a top diameter of 20 μm and an adjacent space of 40 μm (Figure 3(a)). The inset image in Figure 3(b) shows that the height of the micropillars is about 57 μm. The whole surface of the micropillars is covered by abundant hierarchical micro/nano-structures, which originates from the Fe_3O_4 nanoparticles in the SMP composite and the particle ejection during the laser ablation process (Figure 3(b)). If a water droplet was dropped onto the resultant surface, the droplet would spread out quickly with a final CA about 0°. Fluoroalkylsilane modification was utilized to lower the surface free energy of the micropillar array (Figure 1(e)). After fluoroalkylsilane treatment, the CA on the structured Fe_3O_4-SMP composite increased to 153.7° ±1.2° (Figure 3(c)). Water droplets could readily roll off when the surface was inclined by about 7°, revealing low-adhesive superhydrophobicity (Figure 3(c)).

The wettability of the superhydrophobic micropillars can be reversibly converted through regulating the micropillar morphology (Figure 1(f)). Upon heating above T_g, the composite became soft and the micropillar array on the substrate could be easily deformed under the action of an external force. The micropillars were leaned to one side after pressing treatment, as shown in Figure 3(d, e). At this time, the CA on the resultant surface decreased to 140.9°±1° because the increased contact area between the water droplet and the Fe_3O_4-SMP composite (Figure 3(f)). Water droplets could firmly adhere to the sample surface even if the surface was upright or overturned, showing high-adhesive pinning state (Figure 3(f)). Interestingly, the surface morphology of the micropillars could completely restore to stand-up state through NIR light irradiation for about 3–5 s (light intensity: 2.6 W/cm^2, irradiation distance: 30 cm) (Figure 3(a, b)). As a result, the surface re-obtained its original low-adhesive superhydrophobicity (Figure 3(c)). This recovering process is driven by the excellent light-responsive shape-memory ability of the Fe_3O_4-SMP composite. The wettability can also be switched from the high-adhesive pinning state to the low-adhesive sliding state by NIR light even at a long irradiation distance of 2 m, showing strong remote liquid manipulation ability. Moreover, this reversible wettability conversion can be repeated at least 20 times (Figure 3(g, h)). These results indicate that the micropillar-structured Fe_3O_4-SMP composite has extraordinary reversible and controllable wettability.

The switching mechanism of the wettability on the structured Fe_3O_4-SMP composite is illustrated in Figure 4. It is well known that Fe_3O_4 nanoparticle is a kind of photothermal material, which can absorb photon energy and immediately convert it into thermal energy under NIR light irradiation [40–42]. This rapid conversion from photon energy to thermal energy is ascribed to the electron-phonon and phonon-phonon processes of Fe_3O_4 nanoparticles during NIR light irradiation [43]. At room temperature, the molecular chain conformation in the Fe_3O_4-SMP composite is at the thermodynamically stable state [22] (Figure 4(a)). The upright micropillars on the femtosecond laser-structured Fe_3O_4-SMP composite are at the permanent shape. The surface of the micropillars is covered with abundant hierarchical micro/nano-structures (Figure 3(b)). Water droplets can only touch the top portion of the micropillars due to the trapped air cushion between the water droplets and the micropillar-structured Fe_3O_4-SMP composite. At this time, the contact model between the water droplet and Fe_3O_4-SMP micropillar array is a typical Cassie contact state [44] (Figure 4(e)). As a result, the water droplet can slide easily on the sample surface, displaying the low-adhesive superhydrophobicity. When the composite is exposed to NIR light, Fe_3O_4 nanoparticles firstly absorb light and then the surrounding polymer molecules quickly get heated (Figure 4(b)). As the temperature of the Fe_3O_4-SMP composite increases above

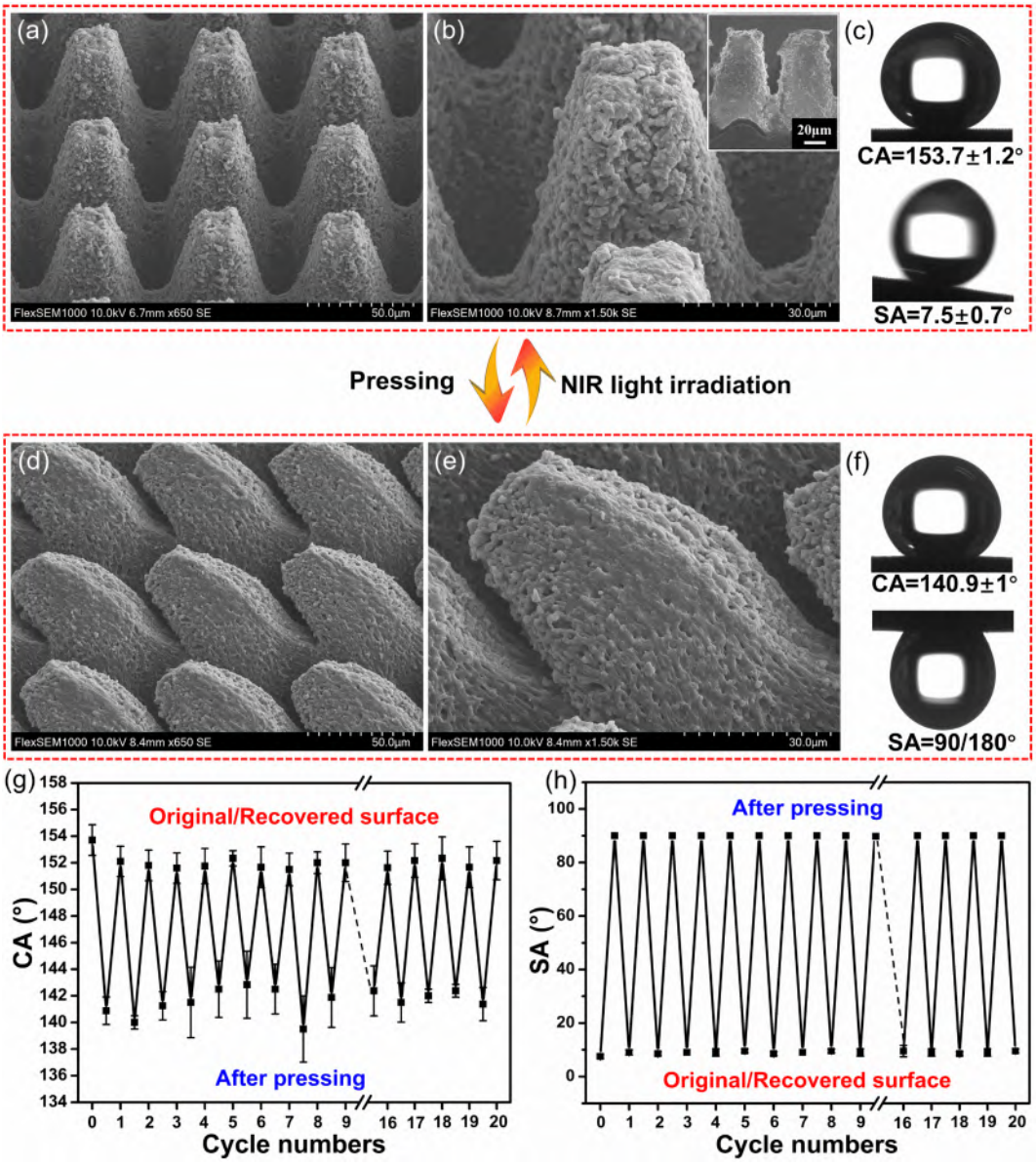

Figure 3 Reversibly switching the surface morphology and the wettability of the Fe_3O_4-SMP micropillars *via* alternate pressing treatment and NIR-light irradiation. (a, b) 45°-tilted SEM images of the original/recovered micropillars on the Fe_3O_4-SMP composite. The inset in (b) is the cross-sectional SEM image of the micropillars. (c) Wettability of a water droplet on the original/recovered sample surface. (d, e) 45°-tilted SEM images of the deformed micropillars. (f) Wettability of a water droplet on the deformed sample surface. Reversible switching of (g) CA and (h) SA with the repeated pressing and NIR-light irradiation processes (color online).

T_g, the molecular chains in the SMP are greatly activated and the composite becomes soft (Figure 4(b)). In this case, the Fe_3O_4-SMP composite can be easily deformed under external pressure (Figure 4(c)). For example, the micropillars can be leaned to one side (Figure 4(f)). Once turning off the NIR light, the composite temperature gradually declines below T_g and the action of SMP molecular chains is largely restricted [22]. The micropillar array is temporarily locked in the deformed morphology (Figure 4(d, f)). When water droplets are dropped on the surface, the water droplet will contact with the most region of the inclined micropillars, not just the top surface of the micropillars. The dramatically increased contact region between the water droplet and the SMP micropillars results in the high-adhesive wettability state. Water droplets would highly adhere to the deformed micropillars even if the sample was vertical or completely overturned, showing high-adhesive pinning state. As a result, the proportion of the air layer embedded between the water droplet and the micropillar array is significantly reduced. The wettability of the surface transformed from the original low-adhesive Cassie state to the high-adhesive Cassie-Wenzel state [45] (Figure 4(f)). Upon returning on the NIR light, Fe_3O_4 nanoparticles will reheat the surrounding polymer molecules, thus facilitating the recovery of surface

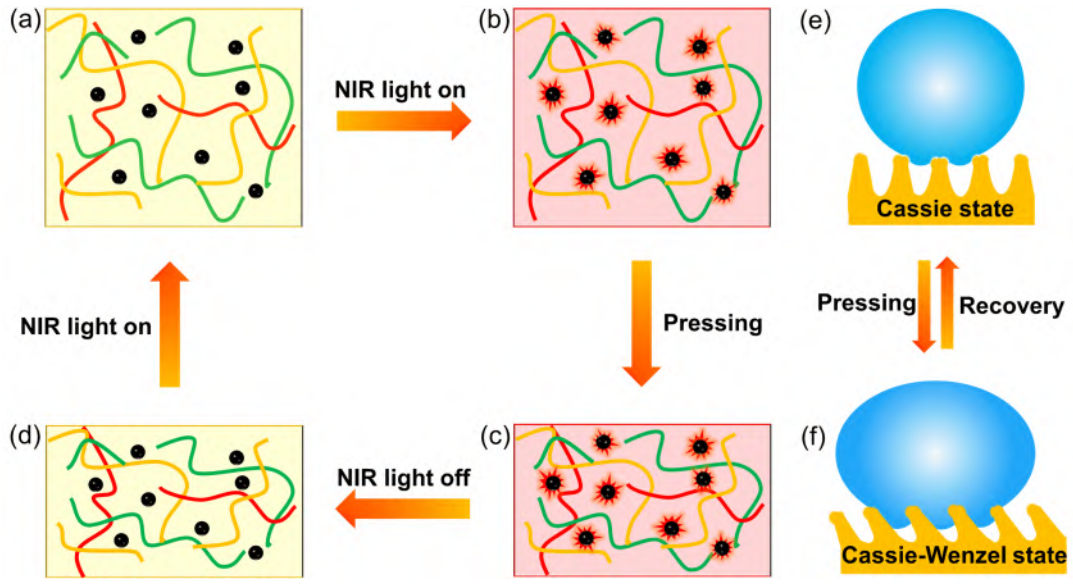

Figure 4 Mechanism of the shape-memory ability and wettability conversion of the Fe_3O_4-SMP composite under NIR light irradiation. Mechanism of the NIR light-triggered shape-memory process of the Fe_3O_4-SMP composite: (a) original Fe_3O_4-SMP molecular crosslinking network, (b) the Fe_3O_4-SMP molecular crosslinking network activated by NIR light, (c) the activated Fe_3O_4-SMP molecular crosslinking network pressed by an external force, and (d) the deformed Fe_3O_4-SMP molecular crosslinking network fixed by cooling. The curved lines represent the molecular crosslinking network of the polymer. The black dots are Fe_3O_4 nanoparticles. Wetting state of a water droplet on (e) the original/recovered Fe_3O_4-SMP micropillars and (f) the deformed Fe_3O_4-SMP micropillars (color online).

morphology and wettability.

3.3 Influence of laser parameters on micropillar morphology and wettability

Femtosecond laser processing is a flexible and effective tool which can design various 3D hierarchical micro/nanostructures on the substrate surface. The height of the as-prepared micropillars can be adjusted by changing the laser power and the interval of scanning lines during laser processing. When the laser power rises from 30, 40, 50, 60, and to 70 mW, the micropillar height increases from 28, 35, 43, 52, and to 60 μm under the constant scanning line interval of 4 μm (Figure 5(a)). Furthermore, the micropillar height almost linearly increases with the laser power, which agrees with the fact that the higher laser power leads to the stronger material removal [46]. With the laser power increasing from 30 to 70 mW, the CA values on the sample surfaces are all above 150° and the SA values are all below 10° (Figure 5(c)). The surfaces with different micropillar heights maintain superhydrophobicity and ultralow water adhesion. The micropillar height gradually decreases with the rise of the interval of scanning lines. When the interval of the scanning lines increases from 2, 4, 6, 8, and to 10 μm, the micropillar height decreases from 57, 35, 30, 20, and to 17 μm under the constant laser power of 40 mW (Figure 5(b)). The decline of micropillar height is owing to the reduction in the number of laser pulses per unit area with the increasing of scanning line interval [47,48]. It can be seen that all the sample surfaces display low-adhesive superhydrophobicity (CA>150°, SA<10°) as the scanning line interval ranges from 2 to 10 μm (Figure 5(d)). The abovementioned results indicate that the micropillar height can be facilely adjusted by changing the laser power and the interval of scanning lines, and the micropillar height has little effect on the surface wettability.

The space between the micropillars is determined by the size of the laser-ablated region while the diameter of the micropillars depends on the size of the untreated region. These two parameters can be freely designed during the laser processing. The influence of the micropillar space on the surface wettability was studied under a constant micropillar diameter of 20 μm and a micropillar height of 35 μm. With the micropillar space increasing from 40, 60, 100, 140, 180, and to 220 μm, the CA values decrease from 153.3°±1.3°, 151.3°±1.7°, 152°±1.8°, 153.8°±0.9°, 150.5°±1.8°, and to 147.3°±0.6°, while the SA values are all below 10° (Figure 5(e)). As the micropillar space increases, the water droplet will be gradually embedded into the intervals of the micropillars. As a result, the contact region between the water droplet and the sample surface increases, which results in a slight decline of CA value. It is indicated that superhydrophobicity can be obtained with the micropillar space ranging from 40 to 180 μm (Figure 5(e)).

Compared to the micropillar space, micropillar diameter has a great effect on the dynamic wettability of the as-prepared surface. As shown in Figure 5(f), when the micropillar diameter increases from 20, 50, 90, 130, and to

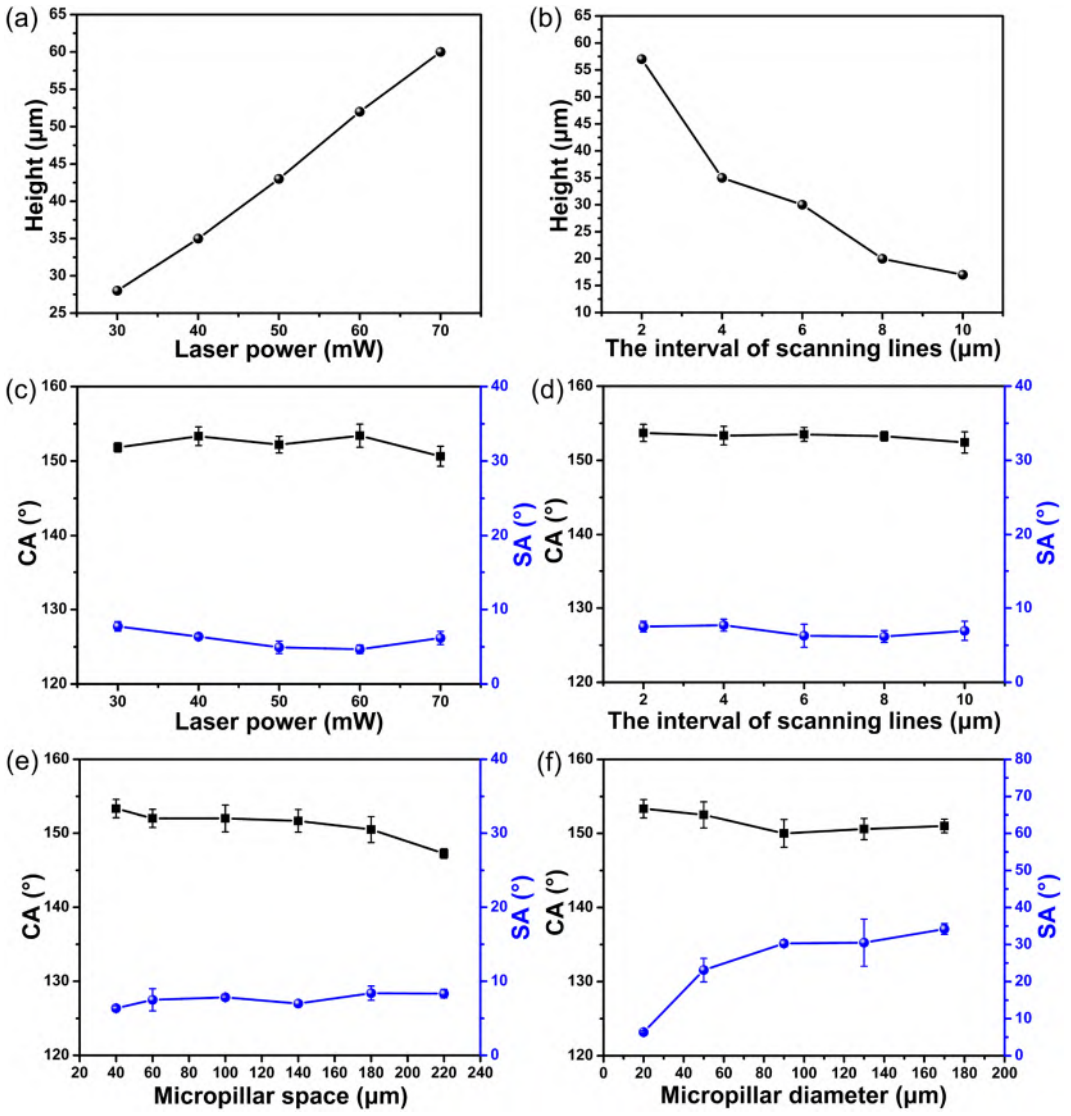

Figure 5 Influence of processing parameters on the surface morphology and wettability. (a) Relationship between the micropillar height and the laser power. (b) Relationship between the micropillar height and the interval of scanning lines. The dependence of surface wettability on (c) the laser processing power, (d) the interval of scanning lines, (e) the micropillar space, and (f) the micropillar diameter (color online).

170 μm (micropillar spacing=40 μm and micropillar height= 35 μm), all the CA values maintain above 150°. However, the SA values obviously increase from 6.4°±0.3°, 23.1°±3.2°, 30.3°±0.9°, 30.5°±6.4°, and to 34.2°±1.4°, indicating that the water adhesion of the surface is gradually increased (Figure 5 (f)). The dramatic increase of water adhesion on the sample surfaces is due to the increase of contact region between the water droplets and the micropillars.

3.4 Light-triggered droplets manipulation

The light-triggered wettability-conversion property enables the as-prepared superhydrophobic Fe_3O_4-SMP surfaces to have the advanced ability of remote droplet manipulation in comparison to the traditional thermal-responsive superhydrophobic SMP surfaces [24,27]. As displayed in Figure 6 (a), a water droplet on the original superhydrophobic micropillar array can easily slide off with a small tilted angle or a slight vibration (Figure 6(b), Movie S1, Supporting Information online). As some micropillars on the sample surface are deformed, such deformed part becomes a high-adhesive region. The water droplet can firmly pin on this region even though the sample is completely overturned (Figure 6(c)). Surprisingly, the captured droplet can be released through NIR light irradiation (Figure 6(d, e)). To demonstrate the *in situ* droplet capture and release process, a 10 μL water droplet was pre-placed on a low-adhesive superhydrophobic substrate (*e.g.*, original superhydrophobic Fe_3O_4-SMP surface). The superhydrophobic Fe_3O_4-SMP surface with deformed micropillars was slowly moved down

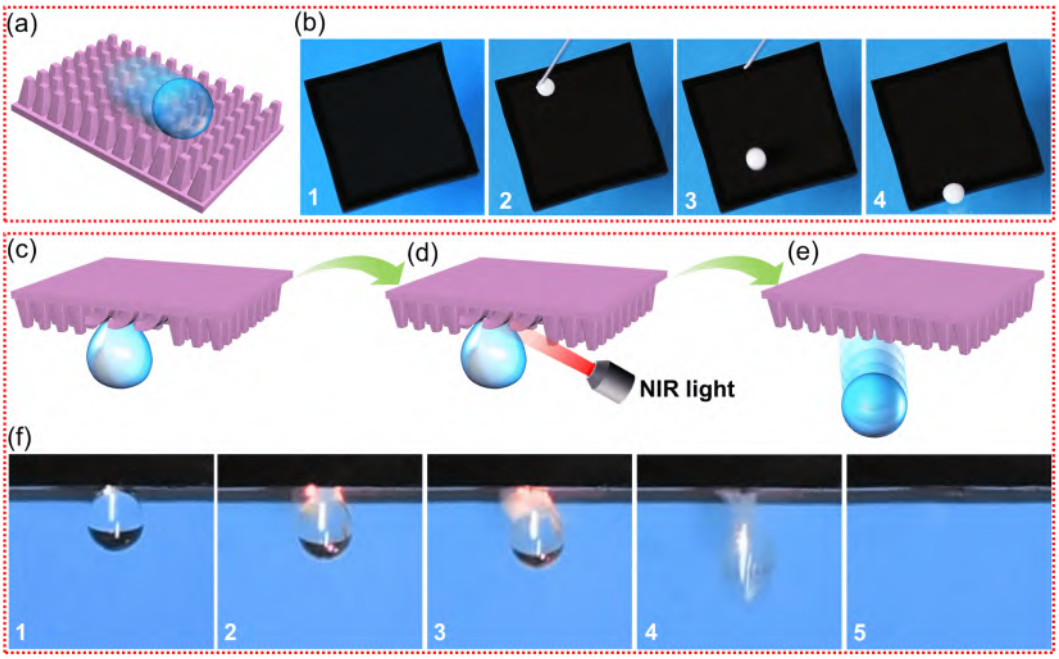

Figure 6 *In situ* droplet release on the Fe_3O_4-SMP micropillar array triggered by NIR light. (a) Illustration of a water droplet rolling on the upright micropillar array. (b) Sliding process of a droplet on the original superhydrophobic Fe_3O_4-SMP micropillars with an inclination angle of 10°. Milk is used here for clear observation. Illustration of the *in situ* release of a droplet through NIR-light irradiation: (c) the droplet pinning on the deformed Fe_3O_4-SMP micropillars, (d) irradiating the region underneath the pinned droplet by NIR light, and (e) the pinned droplet detaching from the sample surface and falling off freely. (f) Time-sequence images of a water droplet (10 μL) detaching from the deformed micropillar array and falling freely triggered by NIR light irradiation (color online).

until it touched the water droplet. Then, the sample was lifted up. Owing to the high water adhesion of the deformed region, the water droplet detached from the original substrate and pinned on the deformed superhydrophobic Fe_3O_4-SMP surface, like being successfully captured by the sample surface. Moreover, the captured droplet could be *in situ* released easily. Once the region underneath the pinned water droplet was irradiated by NIR light (Figure 6(d)), the deformed micropillar array would instantly recover to the original upright state (Figure 6(e)). The contact region between the water droplet and the micropillar array was dramatically decreased. With the recovery of the original low-adhesive superhydrophobicity of the micropillar array, the captured droplet fell off freely from the sample surface (Figure 6(e, f) and Movie S2). In this process, the captured droplets are released through remote light irradiation instead of direct manipulation. This release process can even be triggered by light from a long distance of 2 m. The properties of *in situ* droplet capture and release enable the femtosecond laser-structured Fe_3O_4-SMP micropillar array to have great promise in remote liquid manipulation.

Since the light-irradiated position can be flexibly controlled, thereby causing the selective manipulation of droplet on the Fe_3O_4-SMP micropillar array. As an example, the process of selectively releasing two droplets on one as-prepared superhydrophobic surface is shown in Figure 7 and Movie S3. Two different regions of the micropillars on the superhydrophobic Fe_3O_4-SMP surface were deformed and exhibited high water adhesion by pressing treatment. Two water droplets (A and B) were respectively dispensed onto these two regions and thus tightly adhered to the sample surface in advance (Figure 7(a)). Even if the sample was greatly tilted (*e.g.*, at 65°), the droplets still firmly stuck on the sample surface (Figure 7(e)). The release of either droplet A or B could be realized by selectively irradiating the corresponding region underneath the droplets. For instance, as long as the region underneath the droplet B was irradiated by NIR light (Figure 7(a, f)), the deformed micropillars in this region would immediately recover (Figure 7(b)). With the recovery of ultralow-adhesive superhydrophobicity, the movement of droplet B was triggered and the droplet rolled away the sample surface, achieving rapid release of this droplet (Figure 7(b, g)). The droplet A also could be released like the droplet B. Once the NIR light was switched to irradiate the region underneath the droplet A (Figure 7(c, h)), the movement of the droplet A was also triggered, so this droplet rolled off on the sample surface quickly (Figure 7(d, i, j)). The droplet A could be released first before droplet B through irradiating the region beneath the droplet A first. In addition to releasing two droplets, the surface can also be used to selectively release more droplets. The surface with selective droplets-release property will have important practical values in droplet manipulation technology.

Taking advantage of the remote and selective ability to

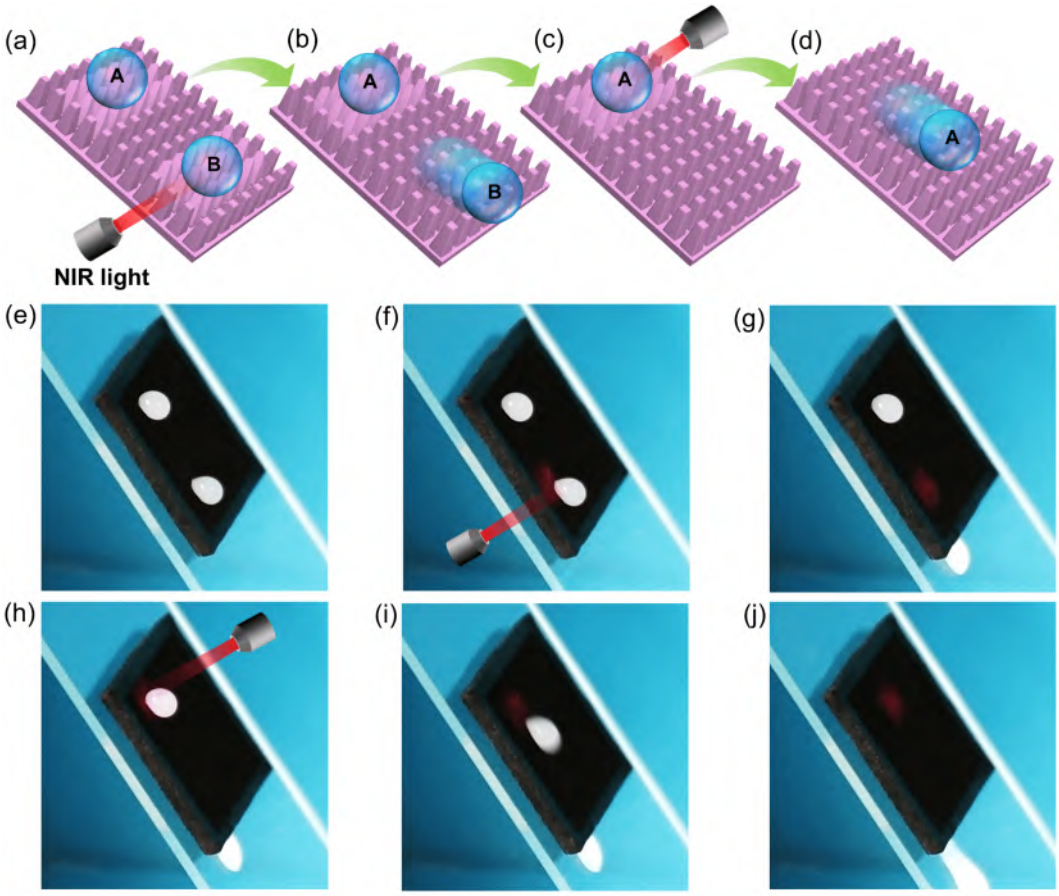

Figure 7 Selective droplet release on the Fe_3O_4-SMP micropillar array controlled by NIR light. (a–d) Illustration of the selective release of droplets *via* NIR light irradiation. (e–j) Time-sequence images of selective releasing a water droplet (10 μL) from the surface tilted at 65°. Milk is used here for clear observation (color online).

manipulate small droplets, the as-fabricated superhydrophobic Fe_3O_4-SMP micropillar array can also be utilized as a platform for achieving droplet coalescence or mergence. As shown in Figure 8(a), two different regions of the micropillars on the superhydrophobic Fe_3O_4-SMP surface were deformed and exhibited high water adhesion by pressing treatment. Two different droplets (A and B) were respectively dropped on two deformed regions on the same sample surface. The droplet A was at the top region of the surface, while the droplet B was at the bottom region. When the NIR light irradiated the region of droplet A, this droplet would slide off on the surface (Figure 8(b)). As the droplet A arrived at the bottom region, the droplet A and B would contact and merge into a larger droplet (Figure 8(c)). Based on this droplet coalescence process, a microreactor was designed on the superhydrophobic Fe_3O_4-SMP micropillar array, as shown in Figure 8(d–i) and Movie S4. A sodium citrate droplet was dropped on the top region of the surface, and a phenol red droplet was dropped on the bottom region (Figure 8(d)). The sample was tilted at about 20°. Once the region underneath the sodium citrate droplet was irradiated by NIR light (Figure 8(e)), this droplet started to roll down (Figure 8(f–h)) and thus met with the phenol red droplet (Figure 8(i)). Finally, the sodium citrate droplet and the phenol red droplet merged into a large droplet. Meanwhile, the color of the merged droplet immediately turned from yellow to red due to the chromogenic reaction between sodium citrate and phenol red (Figure 8(i)). Compared with traditional chemical reaction, the droplet-based microreactor has many advantages including reduced use of chemical reagents, high sensitivity, and low operation cost [49–51]. Such microreactor can also be applied for other chemical reactions, which shows promising prospects in biological detection and chemical synthesis.

4 Conclusions

In summary, a novel superhydrophobic Fe_3O_4-SMP micropillar array with NIR light-triggered reversible water adhesion is prepared by doping Fe_3O_4 nanoparticles into a thermal-responsive SMP material and femtosecond laser processing. The original superhydrophobic Fe_3O_4-SMP micropillar array shows low-adhesive superhydrophobicity

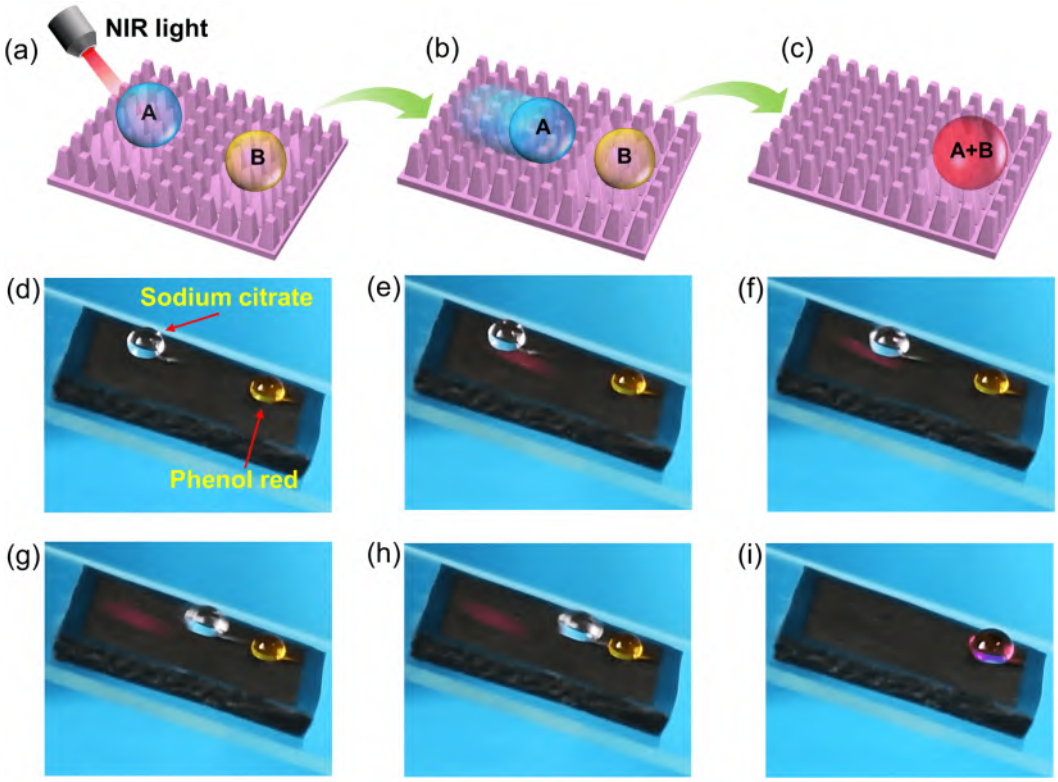

Figure 8 Droplet coalescence on the Fe_3O_4-SMP micropillar array. Illustration of the coalescence of two droplets on the Fe_3O_4-SMP micropillars: (a) droplet A and B pinning on the deformed Fe_3O_4-SMP micropillars, (b) the pinned droplet A starting to roll on the surface by NIR-light irradiating the region underneath the droplet A, and (c) droplet A and B contacting and merging into a larger droplet. Droplet-based microreactor between sodium citrate solution (10 μL) and phenol red solution (6 μL) on the surface of Fe_3O_4-SMP micropillars: (d) the droplets of sodium citrate and phenol red pinning on the deformed Fe_3O_4-SMP micropillars, (e) irradiating the region underneath the sodium citrate droplet by NIR light, (f–h) the process of sodium citrate droplet sliding off on the sample surface, and (i) the reaction between sodium citrate droplet and phenol red droplet after contacting with each other. The surface is tilted at 20° (color online).

with a CA of 153.7°±1.2° and a SA of 7.5°±0.7°. The micropillar array on the Fe_3O_4-SMP composite can be easily deformed (*i.e.*, leaned to one side) by pressing treatment. The sample surface thus switches to high-adhesive state with the water droplets firmly pinning on the sample surface (SA=90°/180°). The NIR light is able to remotely and locally heat the deformed micropillars, and thereby the surface morphology and the wettability are selectively recovered because of the light-responsive shape-memory ability of the Fe_3O_4-SMP composite. This reversible wettability conversion between low-adhesive superhydrophobic state and high-adhesive pinning state can be repeated at least 20 times. Furthermore, the surface enables the wettability to switch from the high-adhesive pinning state to the low-adhesive sliding state by NIR light even at an irradiation distance of 2 m. Compared with previously reported wettability-tunable surfaces, the NIR light-responsive superhydrophobic surface can realize wettability conversion in a remote, selective, and *in situ* manner. Water droplets pinning on the sample surface can be remotely, selectively, and *in situ* released by NIR light irradiation. Taking advantage of the unique NIR light-triggered wettability transformation, the as-fabricated surface can be utilized for lossless liquid transfer, selective liquid release, and droplet-based microreactor. It is anticipated that such surfaces will have promising prospects in liquid manipulation, lab-on-a-chip, and microfluidics.

Acknowledgements This work was supported by the National Key Research and Development Program of China (2017YFB1104700), the National Natural Science Foundation of China (61875158), the International Joint Research Laboratory for Micro/Nano Manufacturing and Measurement Technologies, the Fundamental Research Funds for the Central Universities.

Conflict of interest The authors declare no conflict of interest.

Supporting information The supporting information is available online at http://chem.scichina.com and http://link.springer.com/journal/11426. The supporting materials are published as submitted, without typesetting or editing. The responsibility for scientific accuracy and content remains entirely with the authors.

1 Tang X, Zhu P, Tian Y, Zhou X, Kong T, Wang L. *Nat Commun*, 2017, 8: 14831
2 Tan Y, Hu B, Chu Z, Wu W. *Adv Funct Mater*, 2019, 29: 1900266
3 Chowdhury MS, Zheng W, Kumari S, Heyman J, Zhang X, Dey P, Weitz DA, Haag R. *Nat Commun*, 2019, 10: 4546
4 Han H, Lee JS, Kim H, Shin S, Lee J, Kim J, Hou X, Cho SW, Seo J, Lee T. *ACS Nano*, 2018, 12: 932–941
5 Sun L, Bian F, Wang Y, Wang Y, Zhang X, Zhao Y. *Proc Natl Acad Sci USA*, 2020, 117: 4527–4532

6 Shin S, Lee J, Lee S, Kim H, Seo J, Kim D, Hong J, Lee S, Lee T. *Small*, 2017, 13: 1602865
7 Lehmann U, Vandevyver C, Parashar VK, Gijs MAM. *Angew Chem Int Ed*, 2006, 45: 3062–3067
8 Park JK, Kim S. *Lab Chip*, 2017, 17: 1793–1801
9 Huang CJ, Fang WF, Ke MS, Chou HYE, Yang JT. *Lab Chip*, 2014, 14: 2057–2062
10 Xing S, Harake RS, Pan T. *Lab Chip*, 2011, 11: 3642–3648
11 Lai X, Pu Z, Yu H, Li D. *ACS Appl Mater Interfaces*, 2020, 12: 1817–1824
12 Wu Y, Feng J, Gao H, Feng X, Jiang L. *Adv Mater*, 2019, 31: 1800718
13 Zhang S, Huang J, Chen Z, Yang S, Lai Y. *J Mater Chem A*, 2019, 7: 38–63
14 Ben S, Zhou T, Ma H, Yao J, Ning Y, Tian D, Liu K, Jiang L. *Adv Sci*, 2019, 6: 1900834
15 Zhu S, Bian Y, Wu T, Chen C, Jiao Y, Jiang Z, Huang Z, Li E, Li J, Chu J, Hu Y, Wu D, Jiang L. *Nano Lett*, 2020, 20: 5513–5521
16 Jiang S, Hu Y, Wu H, Zhang Y, Zhang Y, Wang Y, Zhang Y, Zhu W, Li J, Wu D, Chu J. *Adv Mater*, 2019, 31: 1807507
17 Lee WK, Jung WB, Rhee D, Hu J, Lee YAL, Jacobson C, Jung HT, Odom TW. *Adv Mater*, 2018, 30: 1706657
18 Zhang E, Wang Y, Lv T, Li L, Cheng Z, Liu Y. *Nanoscale*, 2015, 7: 6151–6158
19 Liu Y, Gao H, Li S, Han Z, Ren L. *Chem Eng J*, 2018, 337: 697–708
20 Seo J, Lee S, Han H, Jung HB, Hong J, Song G, Cho SM, Park C, Lee W, Lee T. *Adv Mater*, 2013, 25: 4139–4144
21 Wu D, Wu SZ, Chen QD, Zhang YL, Yao J, Yao X, Niu LG, Wang JN, Jiang L, Sun HB. *Adv Mater*, 2011, 23: 545–549
22 Zhao Q, Qi HJ, Xie T. *Prog Polym Sci*, 2015, 49-50: 79–120
23 Habault D, Zhang H, Zhao Y. *Chem Soc Rev*, 2013, 42: 7244–7256
24 Lv T, Cheng Z, Zhang D, Zhang E, Zhao Q, Liu Y, Jiang L. *ACS Nano*, 2016, 10: 9379–9386
25 Chen CM, Yang S. *Adv Mater*, 2014, 26: 1283–1288
26 Wang W, Salazar J, Vahabi H, Joshi-Imre A, Voit WE, Kota AK. *Adv Mater*, 2017, 29: 1700295
27 Bai X, Yang Q, Fang Y, Zhang J, Yong J, Hou X, Chen F. *Chem Eng J*, 2020, 383: 123143
28 Li C, Jiao Y, Lv X, Wu S, Chen C, Zhang Y, Li J, Hu Y, Wu D, Chu J. *ACS Appl Mater Interfaces*, 2020, 12: 13464–13472
29 Li Z, Zhang X, Wang S, Yang Y, Qin B, Wang K, Xie T, Wei Y, Ji Y. *Chem Sci*, 2016, 7: 4741–4747
30 Irajizad P, Ray S, Farokhnia N, Hasnain M, Baldelli S, Ghasemi H. *Adv Mater Interfaces*, 2017, 4: 1700009
31 Chen C, Huang Z, Shi L, Jiao Y, Zhu S, Li J, Hu Y, Chu J, Wu D, Jiang L. *Adv Funct Mater*, 2019, 29: 1904766
32 Zhang F, Xia Y, Liu Y, Leng J. *Nanoscale Horiz*, 2020, 5: 1155–1173
33 Liu L, Liu MH, Deng LL, Lin BP, Yang H. *J Am Chem Soc*, 2017, 139: 11333–11336
34 Jin B, Song H, Jiang R, Song J, Zhao Q, Xie T. *Sci Adv*, 2018, 4: eaao3865
35 He Z, Satarkar N, Xie T, Cheng YT, Hilt JZ. *Adv Mater*, 2011, 23: 3192–3196
36 Shanmugam V, Selvakumar S, Yeh CS. *Chem Soc Rev*, 2014, 43: 6254–6287
37 Chu M, Shao Y, Peng J, Dai X, Li H, Wu Q, Shi D. *Biomaterials*, 2013, 34: 4078–4088
38 Li M, Wang X, Dong B, Sitti M. *Nat Commun*, 2020, 11: 3988
39 Yao X, Jing J, Liang F, Yang Z. *Macromolecules*, 2016, 49: 9618–9625
40 Shang B, Chen M, Wu L. *Small*, 2019, 15: 1901888
41 Zhu CH, Lu Y, Chen JF, Yu SH. *Small*, 2014, 10: 2796–2800
42 Shen S, Wang S, Zheng R, Zhu X, Jiang X, Fu D, Yang W. *Biomaterials*, 2015, 39: 67–74
43 Liu Y, Pei X, Liu Z, Yu B, Yan P, Zhou F. *J Mater Chem A*, 2015, 3: 17074–17079
44 Cassie ABD, Baxter S. *Trans Faraday Soc*, 1944, 40: 546–551
45 Wenzel RN. *Ind Eng Chem*, 1936, 28: 988–994
46 Yong J, Yang Q, Chen F, Zhang D, Farooq U, Du G, Hou X. *J Mater Chem A*, 2014, 2: 5499–5507
47 Yong J, Chen F, Yang Q, Du G, Bian H, Zhang D, Si J, Yun F, Hou X. *ACS Appl Mater Interfaces*, 2013, 5: 9382–9385
48 Yong J, Bai X, Yang Q, Hou X, Chen F. *J Colloid Interface Sci*, 2021, 582: 1203–1212
49 Kim YH, Zhang L, Yu T, Jin M, Qin D, Xia Y. *Small*, 2013, 9: 3462–3467
50 Bannock JH, Krishnadasan SH, Nightingale AM, Yau CP, Khaw K, Burkitt D, Halls JJM, Heeney M, de Mello JC. *Adv Funct Mater*, 2013, 23: 2123–2129
51 Wang Y, Liu S, Zhang T, Cong H, Wei Y, Xu J, Ho YP, Kong SK, Ho HP. *Lab Chip*, 2019, 19: 3870–3879